Journal of Hepatocellular Carcinoma

Dovepress
open access to scientific and medical research

Open Access Full Text Article

ORIGINAL RESEARCH

AGXT2 Suppresses the Proliferation and Dissemination of Hepatocellular Carcinoma Cells by Modulating Intracellular Lipid Metabolism

Tian Chen[1], Lunjian Xiang[2], Wenjin Zhang[3], Zhenyi Xia[4,*], Weixian Chen[1,*]

[1]Department of Laboratory Medicine, The Second Affiliated Hospital of Chongqing Medical University, Chongqing, People's Republic of China; [2]Hepatobiliary Surgery, Chongqing University Three Gorges Hospital, Chongqing, People's Republic of China; [3]Chongqing Municipality Clinical Research Center for Endocrinology and Metabolic Diseases, Chongqing University Three Gorges Hospital, Chongqing, People's Republic of China; [4]Thoracic surgery, Chongqing University Three Gorges Hospital, Chongqing, People's Republic of China

*These authors contributed equally to this work

Correspondence: Weixian Chen; Zhenyi Xia, Department of Laboratory Medicine, The Second Affiliated Hospital of Chongqing Medical University, No. 74 Linjing Road, Yuzhong District, Chongqing, 400010, People's Republic of China, Tel +8613527526490, Fax +86-23-581045783, Email 300801@cqmu.edu.cn; treezhenyi@163.com

Video Abstract

Point your SmartPhone at the code above. If you have a QR code reader the video abstract will appear. Or use: https://youtu.be/N24MIvPCDMQ

Purpose: Alanine glyoxylate aminotransferase (AGXT) family members are crucial in cancer processes, but their role in hepatocellular carcinoma (HCC) metabolism is unclear. This study investigates AGXT2's function in HCC.

Patients and Methods: AGTX2 expression was studied using bioinformatics, real-time reverse transcriptase-polymerase chain reaction (RT-qPCR), Western blot, and Enzyme-linked immunosorbent assay (ELISA). A lentivirus-induced AGTX2 overexpression cell model was analyzed with RNA sequencing (RNA-seq) and liquid chromatography-mass spectrometry (LC-MS). Cholesterol levels were confirmed by Oil Red O staining. AGTX2 effects were evaluated through cell cycle analysis, wound healing, and transwell migration assays.Tumorigenic effects were observed in NOD-SCID IL2Rγnull (NTG) mice in subcutaneous experiments. Protein interaction was examined through co-immunoprecipitation methods.

Results: We observed a significant reduction in AGXT2 mRNA and protein levels in both HCC tumor tissues and serum samples from patients with liver cancer, which was associated with a worse prognosis. The activation of *AGXT2* has been shown to effectively decrease cholesterol levels in liver cancer cells, serving as an antagonist in the cholesterol metabolism pathway. An increase in low density lipoprotein receptor (*LDLR)* mRNA was noted in cells overexpressing AGXT2, accompanied by a decrease in LDLR protein and an elevation in proprotein convertase subtilisin/kexin type 9 (*PCSK9*) mRNA and protein levels. Molecular docking and co-immunoprecipitation experiments further elucidated the interaction between AGXT2 and LDLR proteins. AGXT2 was observed to suppress the migratory and invasive capabilities of HCC cells, inducing cell cycle arrest in the G2/M phase. AGXT2 activation inhibited subcutaneous liver cancer tumor growth in NTG mice.

Conclusion: AGXT2 was found to lower cholesterol levels in liver cancer cells, possibly through interactions with the LDLR protein and modulation of PCSK9-mediated LDLR degradation. This mechanism may impede cholesterol transport to liver cancer cells, thereby suppressing their growth and metastasis.

Keywords: LDLR, PCSK9, cholesterol metabolic, biomarkers

Introduction

Liver cancer ranks as the sixth most prevalent malignancy globally. Approximately 841,000 new cases and 782,000 deaths are reported annually.[1] Hepatocellular carcinoma (HCC) is the final phase of chronic liver disease caused by nonalcoholic fatty liver disease and nonalcoholic steatohepatitis.[2,3] The significant rise in steatosis and nonalcoholic steatohepatitis is a key contributor to the increased risk of HCC development due to metabolic disorders.[4] The worldwide occurrence of HCC is increasing due to its connection with high rates of obesity and type 2 diabetes.[5] Moreover, due to

Received: 2 May 2024
Accepted: 18 August 2024
Published: 24 August 2024

its rapid progression, many patients are found to be in the middle and late stages of the disease, resulting in a poor prognosis. Although some new metabolic therapy drugs have been developed, they have limited effectiveness due to patient specificity,[6] thus necessitating the search for new therapies.

Tumors are seen as a combination of genetic disorders and metabolic disease, with mutations in regulatory genes playing a key role in cancer development and treatment resistance,[7] Recent studies suggest a link between metabolism and epigenetics, which can promote tumor growth. HCC exhibits metabolic changes in genes that support tumor growth and adaptation to harsh environments, with accentuated lipid metabolic reprogramming.[8] Lipid metabolic reprogramming is now a research focus in HCC, in addition to the well-known tumor-promoted glycolysis.[9] Genetic changes in lipid metabolism play a crucial role in liver cancer development, affecting various aspects of the disease.[10] Understanding this connection is essential for finding new targets for effective cancer treatments. High cholesterol increases the risk of liver cancer,[11] but statins can lower cholesterol levels and reduce this risk, particularly in patients with chronic hepatitis B.[12] Research has shown that statins can prevent and treat liver cancer by changing metabolism and immune response in the tumor environment.[13]

However, there is a lack of understanding regarding the regulatory enzymes that either promote or inhibit lipid metabolism in HCC. Alanine glyoxylate aminotransferase 2 (AGXT2), a critical mitochondrial transaminase primarily present in the liver and kidney, exhibits diverse enzymatic activities on substrates, such as Asymmetric Dimethylarginine (ADMA), Symmetric Dimethylarginine (SDMA), and Beta-aminoisobutyric acid (BAIB).[14] Despite its known functions, the involvement of AGXT2 in HCC pathogenesis has not been documented. Our investigation identified varying levels of AGXT2 expression in HCC tissues and blood samples, indicating its potential utility as a biomarker. Furthermore, our findings suggest that AGXT2 may modulate the low density lipoprotein receptor(LDLR), proprotein convertase subtilisin/kexin type 9(PCSK9), and cholesterol metabolic pathways, highlighting its significant role in the lipid metabolism of HCC.

Materials and Methods

Data and Sample Collection

The RNA sequencing (RNA-seq) data and clinical information for 371 patients with liver HCC (LIHC) and 50 adjacent tissues were retrieved from the Cancer Genome Atlas (TCGA) database at https://portal.gdc.cancer.gov/. Additionally, data on healthy liver specimens (n = 110) were obtained from the Genotype-Tissue Expression (GTEx) repository via UCSCXENA (https://xenabrowser.net/datapages/). The RNA-seq data in transcripts per million (TPM) format from TCGA and GTEx underwent standardized processing using the Toil pipeline.[15]

The BioGPS database was used to study AGXT2 expression in healthy human tissues using the U133plus2 Affymetrix microarray. Z-scores were generated using the R software package "frma". A z-score above 5 indicates gene expression in that tissue. BioGPS default settings include lines at the median, 3 times the median, and 10 times the median. On the NCBI website, GEO datasets and input GSE63898[16] were selected in the search box to access AGXT2 expression data from HCC patients and normal liver controls for statistical analysis. Patient consent and ethical approval were obtained for the study, which was conducted at Chongqing University Three Gorges Hospital in China.

Lentivirus Production

The full-length cDNA sequence of *AGXT2* (Gene ID: 64902; Transcript ID: NM_031900.4; CDS length: 1545bp) was cloned from plasmid pHBLV-AGXT2 (Cat.LV002-b, CS5003831, made in Canada, www.abmGood.com, Hanheng Biotech Co. Ltd)., which carried the ZsGreen-PURO viral marker and a 3xflag tag. The AdEasy system was used to create the recombinant Ad-AGXT2 lentivirus, similar to a lentivirus expressing green fluorescent protein and a puromycin selection marker. The Ad-AGXT2 group consisted of pHBLV-CMV-MCS-3FLAG-EF1-ZsGreen-T2A-Puro Lentivirus, whereas the control group consisted of the lentivirus in pHBLV-U6-MCS-CMV-ZsGreen-PGK-Pure-Lentivirus.

Western Blot Analysis

Proteins were separated from cells via electrophoresis using SDS-PAGE and subsequently transferred to PVDF membranes. The membranes were then incubated with primary antibodies targeting AGXT2 (1:7000; Cat. no. 66602-

1-Ig; Proteintech), LDLR (1:800; Cat. no. R380860; Zenbio), PCSK9 (1:800; Cat. no. R25297; Zenbio), angiopoietin like 4 (ANGPTL4) (1:800; Cat. no. R23468; Zenbio), and β-catenin (1:6000; Cat. no. CPA9066; cohesion). Following this, the membranes were exposed to a secondary antibody conjugated with horseradish peroxidase (Abcam). Protein bands were visualized using the Super Signal West Pico Chemiluminescent Substrate Kit from Millipore. β-actin served as the internal control. The experiments were conducted three times separately.

Enzyme-Linked Immunosorbent Assay (ELISA)

The AGXT2 ELISA kit (product no: MB-15972A, lot no. 202112) was purchased from Jiangsu Enzyme Label Biotechnology Co. Ltd. for research purposes only. The kit includes Stop Solution, which changes color from blue to yellow, with color intensity measured at 450 nm using a spectrophotometer. Calibration standards were included to measure the AGXT2 concentration in the samples.

Cell Culture

We used the human epithelial Huh7 cell from the DCTD Tumor Repository (National Cancer Institute, Frederick, MD, USA). Cell lines were grown in DMEM medium (Thermo Fisher Scientific, Waltham, MA, USA) with 10% heat-inactivated fetal bovine serum (Biosera, Boussens, France) and penicillin/streptomycin (Solarbio, P1400) in a humidified incubator at 37°C with 5% CO_2. Both types of cells were placed in 6-well dishes and grown until they reached sub-confluency, which is defined as less than or equal to 80% culture dish coverage. Each cell culture experiment was conducted three times.

RNA Sequencing

Huh7 cells were infected with Ad-AGXT2 for 48 h before RNA-seq. RNA was isolated using TRIzol, and RNA-seq studies were conducted using Panomix, ShuZhou. Oligo(dT) magnetic beads were used to enrich mRNA-containing total RNA. 300 bp fragments were selected using ion disruption, and cDNA was synthesized from RNA using random primers and reverse transcriptase. The second cDNA strand was created using the initial cDNA strand as a guide, followed by PCR amplification to increase the library size to 450 bp. The library was then analyzed for concentration and quality using the Agilent 2100 Bioanalyzer before blending libraries with different index sequences based on their concentration and data requirements. The library was diluted to 2 nM, denatured, and sequenced using NGS technology on the Illumina HiSeq platform.

Differential Gene Expression Analysis

We compared gene expression between the overexpressing group and the control group using DESeq to identify differentially expressed genes with an absolute log2-foldchange > 1 and a p-value < 0.05. We visualized the results with volcano plots, Venn diagrams, and an annular heatmap using ggplot2.[17]

Gene Ontology and Pathway Analysis

Gene ontology (GO) annotations were gathered from diverse sources, and significant categories were identified through the application of Fisher's exact test with false discovery rates (FDR) correction. Pathway analysis was carried out utilizing the Kyoto Encyclopedia of Genes and Genomes (KEGG) database to ascertain crucial pathways associated with differentially expressed genes. Fisher's exact test was employed to detect noteworthy pathways, with significance assessed based on both the p-value and the FDR threshold. Functional enrichment analysis was executed using Gene Set Enrichment Analysis (GSEA), GO, and KEGG, along with progeny enrichment analysis facilitated by the R packages "fgsea", "clusterProfiler", and "progeny".

Reverse Transcription (RT)-PCR and Real-Time PCR

Transfected cells were lysed using TRIzol (Takara). The RNA was subjected to reverse transcription using All-In-One 5X RT MasterMix from abm (Cat. No. G592). BlasTaqTM 2X qPCR MasterMix (abm, Cat. No. G891) was utilized to measure the expression levels of specific genes in a real-time fluorescent quantitative PCR assay system (qTower2.2, 313BO305, Jena, Germany). Relative expression was determined by comparing the transcription level to the expression of *GAPDH*. Invitrogen synthesized the primers, which can be found in Table 1.

Table 1 The Primers Used for qPCR Analysis

Gene	Gene Primer Sequence (5′-3′)
AGXT2	F: TCCCGGACATCAGTAACCAAG R: ACTGGTATCTTTCAGGCATGAAG
LDLR	F: TCAAGTGTCACAGCGGCGAATG R: GTTGGTGAAGAAGAGGTAGGCGATG
PCSK9	F: GAGGACGGCGACTACGAGGAG R: CTGAGGCAGGAGAACCACTTGAAC
GAPDH	F: TGTTTCCTCGTCCCGTAGA R: ATCTCCACTTTGCCACTGC
Si-NC	F: UUCUCCGAACGUGUCACGUdTdT R: ACGUGACACGUUCGGAGAAdTdT
Si-AGXT2	F: CCUGAAAGAUACCAGUCCCUU tt R: AAGGGACUGGUAUCUUUCAGG tt

Histological and Immunohistochemistry

Liver samples were fixed in 4% paraformaldehyde and processed for histological analysis by embedding them in paraffin. Subsequently, the samples were sectioned into 4.5 mm slices and prepared for staining with hematoxylin and eosin (H&E) or immunohistochemistry (IHC) using antibodies targeting AGXT2 (1:1000) and β-catenin (1:500). For the IHC procedure, the samples were incubated with a secondary antibody against rabbit IgG (ZSGB-BIO, Beijing, China) and visualized with 3.30-diaminobenzidine (ZSGB-BIO). Slides were scanned using a Pannoramic Scan 250 Flash or MIDI system, and pictures were captured with Pannoramic Viewer 1.15.2 (3DHistech, Budapest, Hungary).

Ultra-High Performance Liquid Chromatography-Tandem Mass Spectrometry (UPLC-MS/MS)

The samples were thawed at 4°C. Then, 100 mg was transferred to a 2 mL centrifuge tube. The specimen was sonicated with 0.3 mL of ethanol at 25°C for 30 min and centrifuged at 12,000 rpm for 10 min. The supernatant was filtered through a 0.22 μm membrane and examined using UPLC-MS/MS from BioNovoGene. A quality criteria sample was made by combining 30 μL of filtrate from each supernatant. Quality assurance samples were utilized to track the variation in the analysis outcomes of the combined sample blends and to contrast this variation with the analyzer's inherent error. UPLC-MS/MS was used to test the remaining samples.[18,19]

Combined Transcriptome and Metabolome Analysis

Metabolome and transcriptome data are integrated to analyze metabolism and transcription. This involves comparing metabolite and mRNA levels, identifying correlations between metabolites and genes, and creating a network to pinpoint key genes affecting metabolite changes. Enriched KEGG pathways are also examined to understand the relationship between metabolites and genes, providing a comprehensive view of biological processes.

Oil Red O Stain

During setup, a glass shard was placed in a 6-well dish, cells were grown to 80% confluence, and plasmid and siRNA were added. After 48 h, the oil red O test was stained using a kit from Solarbio (G1262). The cells were then washed with PBS, fixed with red O fixative and oil for 20–30 min, washed with distilled water, soaked in 60% isopropyl alcohol, and then stained with oil red O dye solution. Remove the colorant and wash with 60% isopropyl alcohol until the cells are transparent. Rinse, stain nuclei with Mayer's hematoxylin, rinse again, apply oil red O buffer for 1 min, and then observe under a microscope after adding distilled water.

SiRNA Transfection

The siRNA (from GeneBiogist in Shanghai, China, with gene ID 64902) was diluted in RNase-free water to a concentration of 40 nM and then refrigerated at 4°C. Lipofectamine 3000 from Thermo Fisher was thinned in Serum-free medium (diluted at a ratio of 1:50) and kept at room temperature. The siRNA was combined with the transfection agent in the solution. After 24 h, the cells that had been transfected successfully were recognized. The siRNA sequences are listed in Table 1.

Plasmid Transfection

The AGXT2 overexpression plasmid and control vector were purchased from the MiaoLing Plasmid Platform in Hubei, China. Cells were transfected with Lipofectamine 3000 following the manufacturer's instructions. Transfection was done in serum-free medium and switched to serum-containing medium after 6 h for continued culture.

Protein–Protein Molecular Docking

The first step involved searching the UniProt database for human AGXT2 and LDLR proteins. AGXT2's structure was predicted using alphafold2, while LDLR prediction used a 1IJQ structure. Various operations were performed on the proteins, including bond distribution, hydrogenation, and optimization of the hydrogen bond network. The optimized potentials for liquid simulations (OPLS) force field was used to minimize protein energy before molecular docking with the Schrödinger Piper module. Docking was performed in standard mode with 70,000 rotatable probes for the ligand and 30 conformational samples generated. Only one strand was used for docking proteins with multiple strands. Piper grouped the first 1000 rotational conformations by RMSD and selected representative conformations with the most neighbor in each class. The resulting conformations were ranked based on the number of clusters, with those with the most clusters selected for further analysis.

Co-Immunoprecipitation

The co-immunoprecipitation assay was conducted using the Pierce^{TM} Classic Magnetic Bead method, as outlined in the co-immunoprecipitation Kit manufactured by Thermo Scientific (item no. 88804, REF 1861603, lot no. XL358320, USA). Cultured cell lysate was incubated with a specific antibody for immunoprecipitation for either 1–2 h at room temperature or overnight at 4°C. The antigen/antibody complex was then bound to Protein A/G magnetic beads and incubated for 1 h at room temperature. The beads were then washed twice with IP Lysis/Wash Buffer and once with distilled water before the separation of the antigen/antibody complex.

Transwell Assays

An 8-μm pore transwell compartment from R&D Systems was used for migration and invasion tests. A total of 50,000 cells were added to the top chamber without serum, while a serum-containing medium was added to the lower chamber. Matrigel was used for the invasion tests. After a 24-h incubation, the cells were stained with crystal violet and analyzed.

Scratch Test Assay

Huh7 cells were grown in 6-well plates until almost fully grown. The cells were then scraped off gently and rinsed with serum-free medium. The remaining cells were observed for migration progress at 0 h and 48 h.

DNA Content Quantitation Assay (Cell Cycle)

The cells were transfected with *AGXT2* plasmid and siRNA, followed by collection and centrifugation. The cells were then fixed with 70% ethanol for 2 h or overnight at 4°C. The solution was washed with PBS before staining. Cells can be filtered if necessary. They were treated with RNase A and PI dye and then incubated at 37°C for 30 min. After incubation at 4°C for 30 min in the dark, red fluorescence was detected by computer at 488 nm.

Experiment of Subcutaneous Tumor Formation in NOD-SCID IL2Rγnull (NTG) Mice

Fourteen 4-week-old NTG mice (SiPeiFu, Beijing, SCXK2019-0010) were divided into two groups, each consisting of seven mice. The overexpression group received injections of Huh7 cells transfected with overexpressed lentivirus (phblv-adAGXT2) subcutaneously under the armpit, while the control group received unilateral axillary subcutaneous injections of blank Huh7 cells. The mice were observed for a period of 28 days. The mice experiments were performed in accordance with the "Guide for the Care and Use of Laboratory Animals" of the National Institute of Health in China and approved by the Ethics Committee of Chongqing University Three Gorges Hospital (file number: SXYYWD2023).

Quantification and Statistical Analysis

Each cell and biochemical assay was repeated a minimum of three times to ensure robust and conclusive results, while human tissue experiments were replicated twice. Data analysis was performed using SPSS 29.0 and GraphPad Prism 8 to compare the outcomes across the various groups. Statistical analyses included the two-tailed Student's *t*-test for pairwise comparisons, one-way ANOVA with Tukey's post-test for single-variable assessments, two-way ANOVA with Bonferroni's post-test for dual-variable analyzes, and the Pearson coefficient for evaluating linear correlations between variables. We use the normality test of the data distribution to evaluate whether the data conforms to the hypotheses of the statistical test. Statistical parameters are located in the figure captions, with values below 0.05 deemed statistically significant.

Results

Expression Profile of AGXT2 at the mRNA Level Based on TCGA, BioGPS, GTEx, GEO Database, and HCC Patients

We investigated *AGXT2* mRNA expression levels in diverse human tumor types by interrogating the TCGA database. *AGXT2* exhibited significantly diminished expression in several tumor tissues, including liver hepatocellular carcinoma (LIHC), cholangiocarcinoma (CHOL), kidney chromophobe (KICH), kidney renal clear cell carcinoma (KIRC), and kidney renal papillary cell carcinoma (KIRP). However, we found no substantial differentiation of the gene in numerous other tumor types. These findings imply that *AGXT2* may have varying implications for the pathogenesis of liver and kidney tumors (Figure 1A). We employed the BioGPS database to examine *AGXT2* mRNA expression levels in various normal human tissues. *AGXT2* demonstrated significantly elevated expression in the kidney, kidney cortex, kidney medulla, and liver. Other tissues exhibited low levels of *AGXT2* expression (Figure 1B). The levels of *AGXT2* mRNA exhibited a significant decrease in HCC when compared to normal liver tissues, as evidenced by data from TCGA and GTEx databases ($p < 0.001$, Figure 1C). GSE63898 data also indicated a significant decrease in *AGXT2* mRNA levels in HCC tissues when compared to normal liver tissues ($p < 0.001$, Figure 1D). The expression of *AGXT2* gene mRNA was significantly downregulated by real-time reverse transcriptase-polymerase chain reaction (RT-qPCR) in 32 cases of HCC ($p < 0.001$, Figure 1E).

The Expression of AGXT2 Was Downregulated in HCC Tissues and Serum

AGXT2 has the potential to serve as a diagnostic marker for HCC in pathological assessments. Western blot analysis showed a notable decrease or lack of AGXT2 protein expression in the cancer tissues of 12 HCC patients compared to the adjacent liver tissues, with a significant value of $p = 0.0011$ (Figure 2A and B). AGXT2 protein expression was also significantly downregulated in the sera of 40 patients with liver cancer, as detected by ELISA, compared to the sera of 40 normal persons (Figure 2C). We conducted IHC staining on a tissue microarray containing 40 human primary liver tumors and corresponding normal liver tissues to investigate the presence and clinical significance of AGXT2 in HCC. Interestingly, we discovered a notable decrease in AGXT2 expression in human liver tumors compared to nearby normal liver tissues. Specifically, it was feasible to differentiate tumor tissue from neighboring normal tissue visually (Figure 2D). Under a microscope, we could clearly distinguish liver cancer tissue from adjacent tissue (Figure 2E and F).

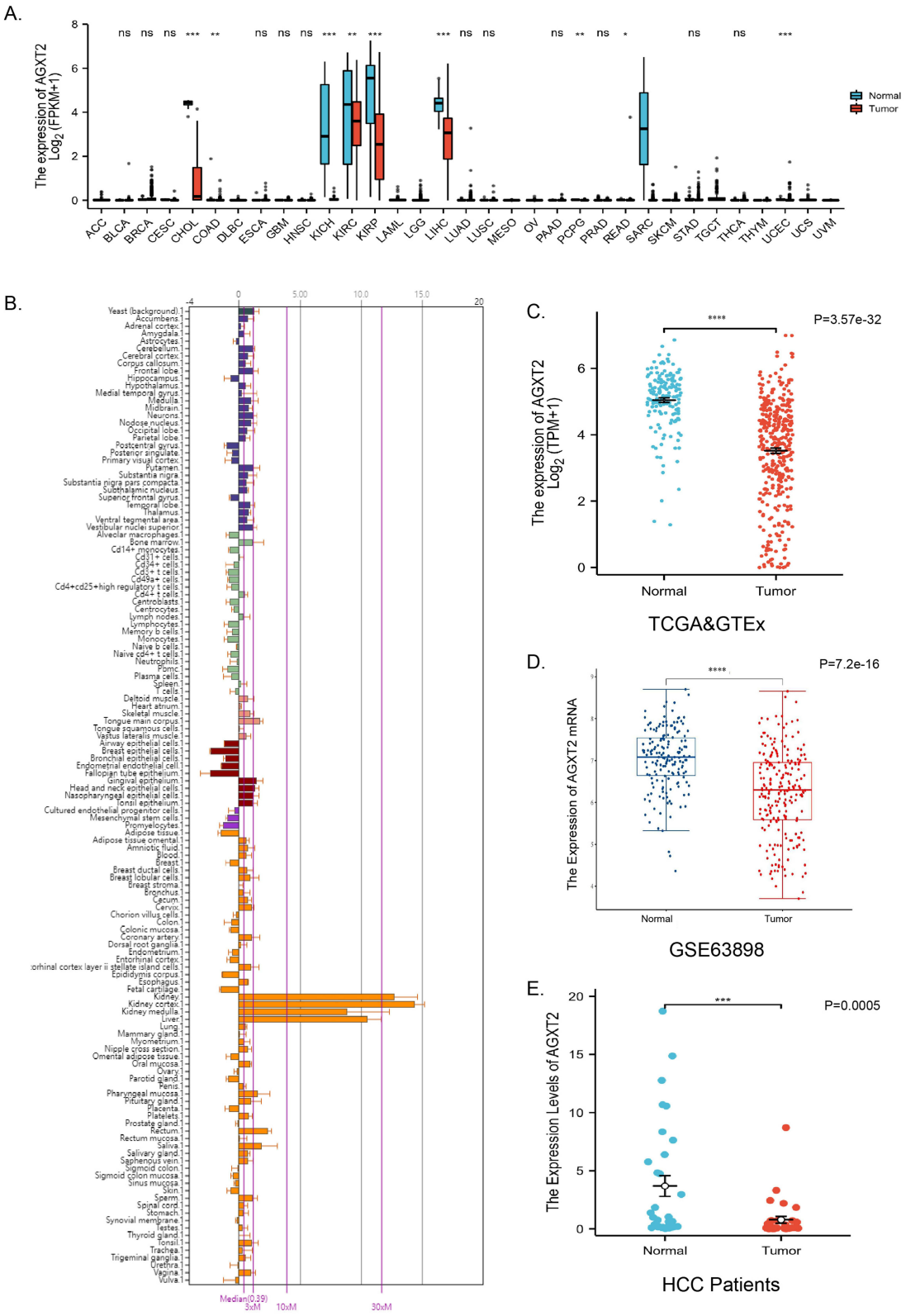

Figure 1 Expression profile of AGXT2 at the mRNA level. The expression of the AGXT2 gene was analyzed across various cancer types and specific subtypes utilizing datasets from TCGA. (**A**) The BioGPS database indicates that AGXT2 is predominantly expressed in liver and kidney tissues. (**B**) Analysis of TCGA and GTEx datasets revealed a significant decrease in AGXT2 mRNA expression in HCC tissues compared to normal liver tissues. (**C**) AGXT2 expression was significantly lower in HCC tissues compared to normal liver tissues in the GSE63898 dataset. (**D**) Among a cohort of 32 patients with HCC, there was a notable decrease in AGXT2 gene mRNA expression. **Notes**: Significance levels are denoted as follows: *$p \leq 0.05$, **$p \leq 0.01$, ***$p \leq 0.001$.

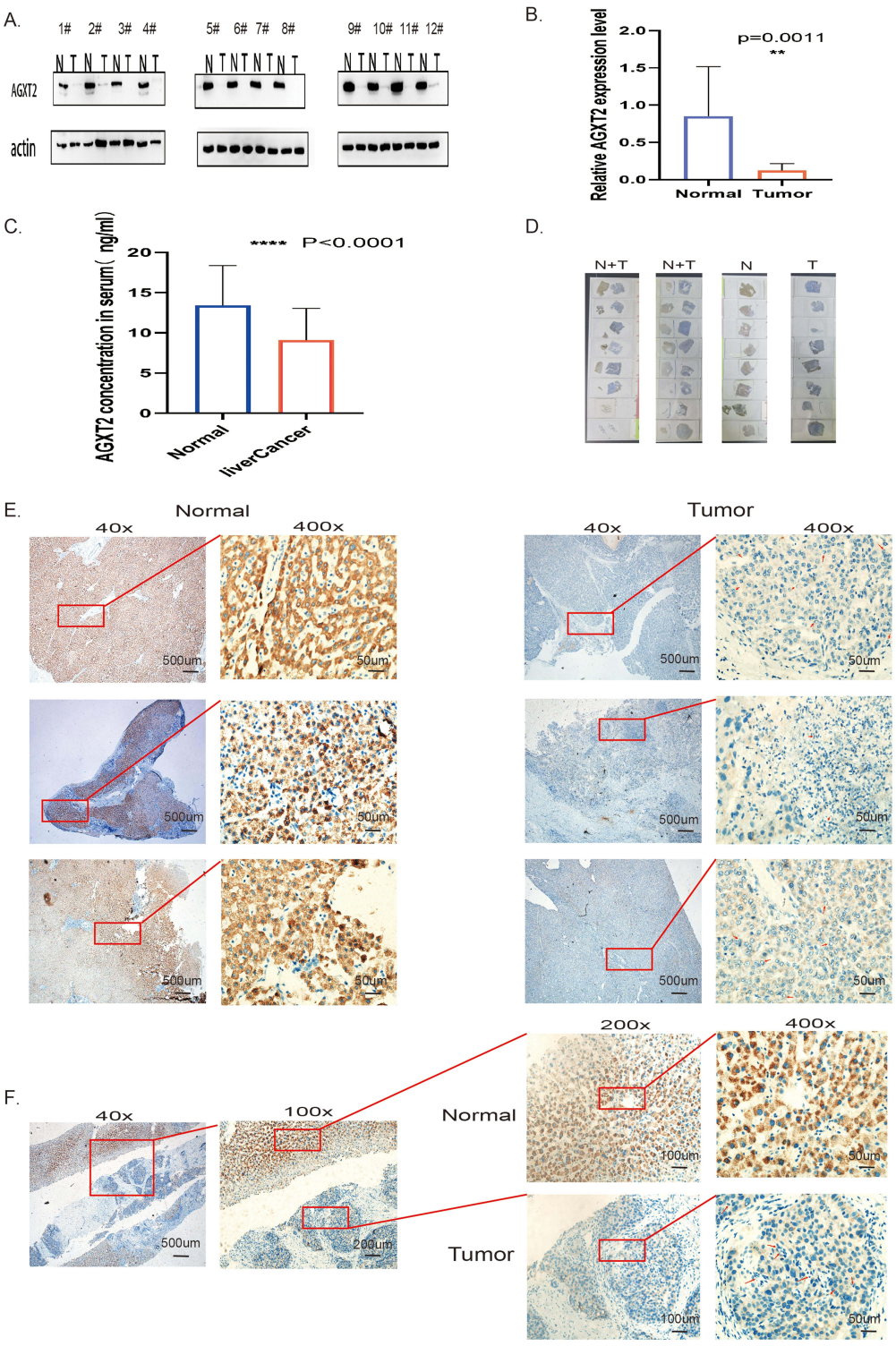

Figure 2 Expression of AGXT2 protein in HCC tissues and serum.(**A**) The AGXT2 gene expression status in tumor tissue (**T**) and adjacent normal tissue (**N**) of HCC was analyzed using Western blot assay. (**B**) Statistical analysis of AGXT2 protein levels in 12 pairs of human liver tumors and adjacent normal liver tissues was conducted through Western blot. AGXT2 protein levels were quantified using Images J software. (**C**) AGXT2 protein expression in the sera of 40 patients with liver cancer was assessed by ELISA. (**D**) Tumor tissue (**T**) and adjacent normal tissue (**N**) were visualized using IHC staining for observation. (**E**) The immunohistochemical staining technique was utilized to detect the expression level of AGXT2 protein in 40 pairs of human liver tumors and their corresponding adjacent normal liver tissues. A subset of four pairs of specimens were randomly selected for inclusion in the figure depicting AGXT2 immunohistochemical staining. (**F**) The immunohistochemical results of AGXT2 in a biopsy specimen from a liver cancer patient were examined.

Notes: Significance levels are denoted as follows: *$p \leq 0.05$, **$p \leq 0.01$, ***$p \leq 0.001$).

RNA-Seq Data and UPLC-MS/MS Data Analysis from Huh7 Overexpressing AGXT2

Initially, we established an AGXT2-overexpression model in Huh7 cells through infection with Ad-AGXT2 and Ad-GFP. RNA-Seq analysis was performed on extracted total RNA to identify differentially expressed genes (DEGs). Over 92.51% of Q30 bases were present, and the alignment rate of clean reads with the specified reference genome fell between 94.02% and 94.48%. A total of 15481 genes were detected. The heat map created with the DEGs showed that 415 genes were upregulated and 345 genes were downregulated in the cells with AGXT2 overexpression (Figure 3A). Using the AGXT2-overexpression model, we examined the 60 most differentially expressed genes. There were notable increases in expression levels of the genes such as *AGXT2, CASP14, HSPA1B, HSPA8, EGLN3, HSPA1A, COL6A2*, and *ANGPTL4*, while genes such as *FGF21, CHAC1, CTH, UNC5B, ATF3, PSG4*, and *CLDN1* showed significant decreases (Figure 3B). The genes controlled by *AGXT2* are closely associated with biological function and strongly linked to tumorigenesis. To understand the varying status of DEGs, we employed a volcano plot to display the gene expression level on the horizontal axis and the differences in gene expression between groups on the vertical axis, as depicted in Figure 3C. We then identified differentially expressed transcripts (DETs) in the AGXT2 overexpression model. The combined number of metabolites identified in the Ad-AGXT2 and Ad-GFP analyses was 261, as illustrated by the differential expression tags visualized in a heatmap (Figure 3D). The total number of differential metabolites was 42 DETs (Figure 3E). Some of the DETs exhibited distinguished transcriptome profiles (17 upregulated and 25 downregulated DETs) (Figure 3F). Following AGXT2 gene overexpression in Huh7 cells, cholesterol was most significantly downregulated in metabolites (Log FC = −7.01, p = 0.0129) (Figure 3G).

AGXT2 Regulates Intracellular Cholesterol Levels by Affecting LDLR and PCSK9

We performed a KEGG pathway enrichment joint analysis using DEGs and DETs. Lipid and atherosclerosis pathways were the most significant (p = 8.63E-07). Cholesterol metabolic pathways can influence the source and transport levels of cholesterol. Consequently, to understand the mechanism of AGXT2 regulation of cholesterol, we chose to study the cholesterol metabolic pathway (Figure 4A). We intersected 51 genes of the cholesterol metabolic pathway with the top 500 DEG genes of the overexpressing AGXT2. We obtained three intersecting genes: *ANGPTL4* (Log2FC = 2.29, p = 3.366E-29), *LDLR* (Log2FC = 1, p = 8.649E-13), and *PCSK9* (Log2FC = 1.78, p = 2.654E-07) (Figure 4B). According to the cholesterol metabolism pathway map, *ANGPTL4* mainly regulates extracellular triglyceride and fatty acid metabolism in the liver. Therefore, we focused on *LDLR* and *PCSK9* and verified the upregulation of *LDLR* mRNA and *PCSK9* mRNA by RT-qPCR. We found the results consistent with the seq-RNA results (Figure 4C). An experiment using oil red O staining was performed to identify the increased expression of AGXT2 plasmid and alterations in lipid droplets following siRNA knockdown in Huh7 HCC cells. Different interventions of the *AGXT2* gene were divided into five groups: overexpressed plasmid Ad-AGXT2 group, no-loaded pcDNA3.1 group, siRNA-AGXT2 group, siRNA-NC group, and control group. We found that lipid droplets increased after AGXT2 knockdown (p = 0.0001) and decreased after AGXT2 overexpression (p = 0.0179) (Figure 4D). Protein–protein docking computer software analysis showed that AGXT2 protein and LDLR protein had six hydrogen bonds and one salt bridge (Figure 4E). Subsequent to AGXT2 overexpression, the protein levels of LDLR were downregulated, while those of PCSK9 were upregulated. Conversely, there was no significant variance in ANGPTL4 protein expression (Figure 4F). A plasmid encoding the AGXT2-3HA tag was constructed and transfected into 293T cells. A co-immunoprecipitation experiment was carried out, revealing the binding of the AGXT2 protein to the LDLR protein (Figure 4G).

AGXT2 Inhibits the Growth and Spread of Tumors in Living Organisms and in vitro

Huh7 cells were incubated with SiRNA-AGXT2 and Ad-AGXT2 for 48 h to activate or inhibit AGXT2 expression, respectively. The migration ability of the cells was detected using the scratch test. A transwell migration assay was used to detect the invasion ability of the cells and statistically analyzed using ImageJ computer software. The scratch assay results showed a significant increase in the proportion of wound healing after AGXT2 inhibition, while it was significantly decreased after AGXT2 upregulation (Figure 5A). The statistical analysis results obtained from ImageJ and GraphPad revealed a significant disparity in the proportion of cells participating in the process of wound healing

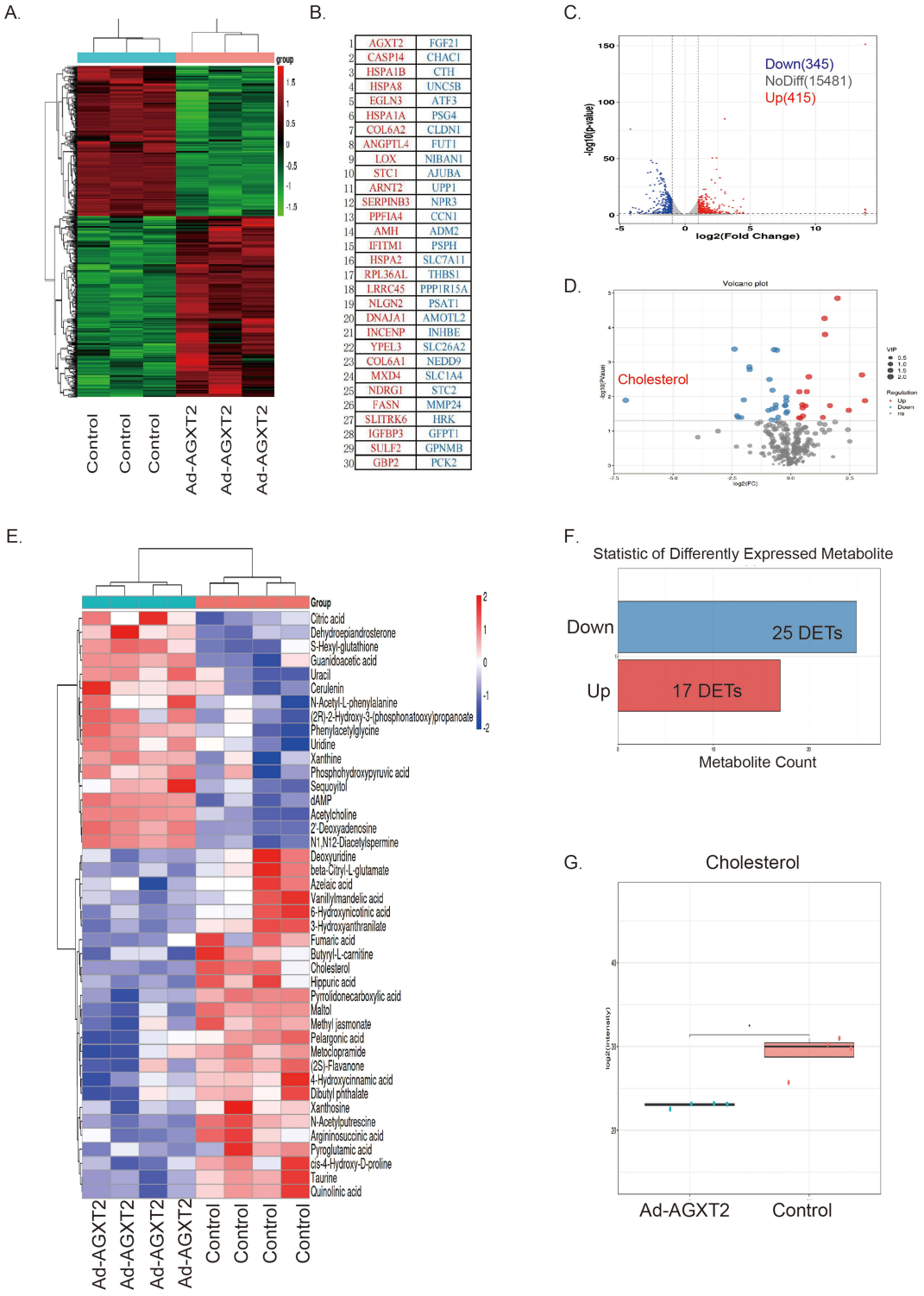

Figure 3 RNA-Seq data and LC-MS data analysis from the AGXT2-overexpression model.(**A**) Utilizing a heat map as a visual representation to illustrate the DEGs across multiple datasets. The heat map employs a color gradient to indicate the level of transcript enrichment, with red denoting upregulated genes and green denoting downregulated genes. (**B**) Identifying the top 60 genes exhibiting variance in expression levels attributed to AGXT2, with red representing upregulation and blue representing downregulation. (**C**) Volcano plot displaying genes that are expressed differentially in DEGs. The log2 fold change difference associating with the Control and Ad-AGXT2 samples is showed on the x - axis, and negative log of *p* - values is showed on the *y* - axis. Every point represents a gene that has measurable expression in both samples. (**D**) Volcano plot of DETs in Huh7 cell with the AGXT2-overexpression. (**E**) Visualization of DETs using a heat map across various sample data sets. Red indicates the transcripts that are upregulated in the heatmaps, while blue indicates the downregulated transcripts. F. Statistics of 17 upregulated and 25 downregulated DETs. (**F**) Cholesterol was most significantly downregulated in metabolites (Log FC = −7.01, $p = 0.0129$).

Notes: Significance levels are denoted as follows: *$p \leq 0.05$, **$p \leq 0.01$, ***$p \leq 0.001$.

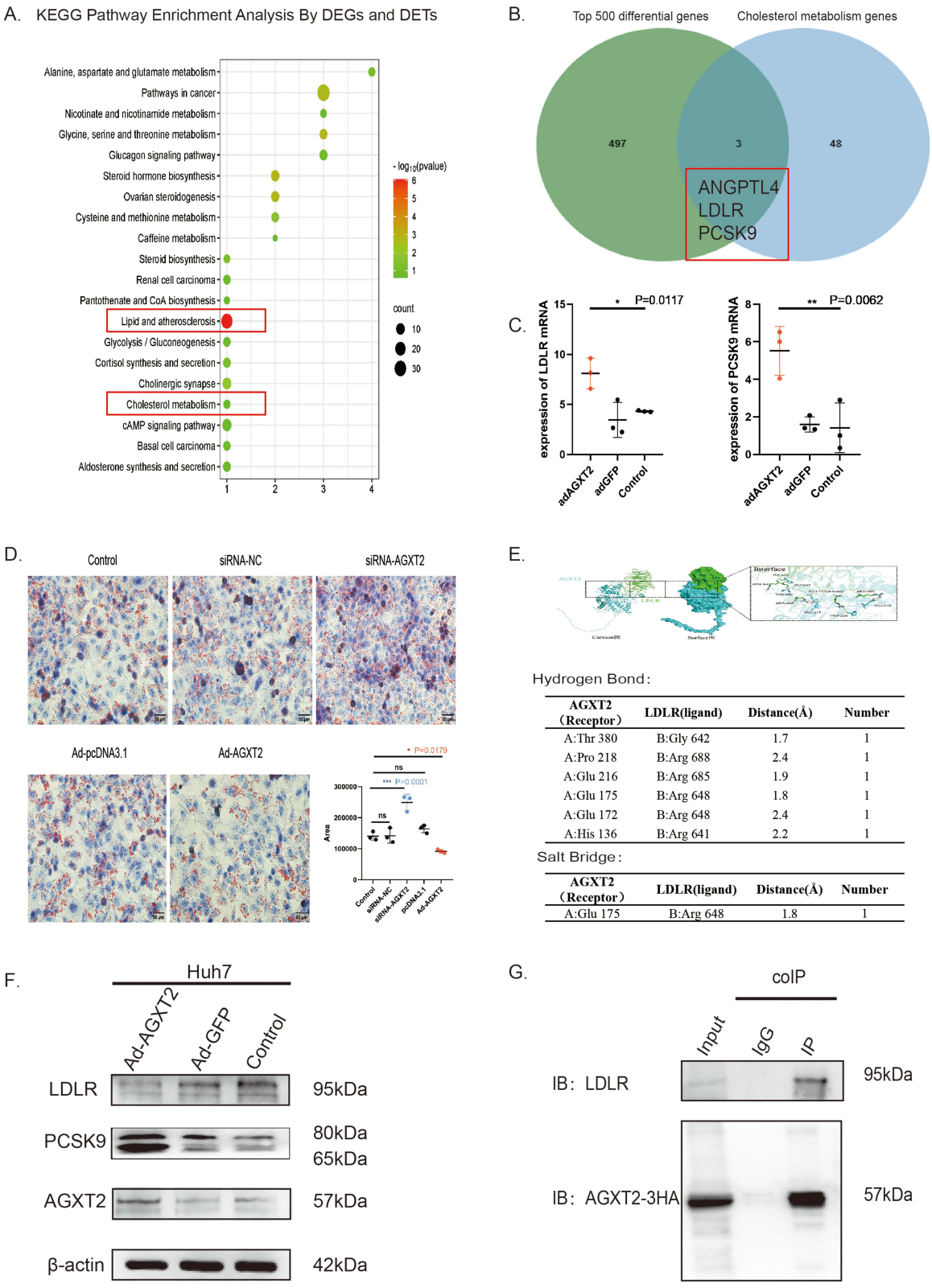

Figure 4 AGXT2 regulated the cholesterol level of liver cancer cells by down-regulating LDLR.(**A**) KEGG pathway enrichment joint analysis by DEGs and DETs. (**B**) Intersected 51 genes of the cholesterol metabolic pathway with the top 500 DEGs genes of overexpressing AGXT2. (**C**) *LDLR* and *PCSK9* mRNA were increased after AGXT2 overexpression. (**D**) AGXT2 reduces intracellular cholesterol levels in liver cancer by an oil red O staining. (**E**) Protein-protein molecular docking technique predicted that AGXT2 and LDLR had 6 bonding hydrogen bonds and 1 salt bridge. (**F**) Ectopic expression of AGXT2 induced LDLR protein level and increase PCSK9 protein level which were detected by Western blotting. (**G**) AGXT2 protein is bound to LDLR protein by co-immunoprecipitation.
Notes: Significance levels are denoted as follows:*$p \leq 0.05$, **$p \leq 0.01$, ***$p \leq 0.001$.

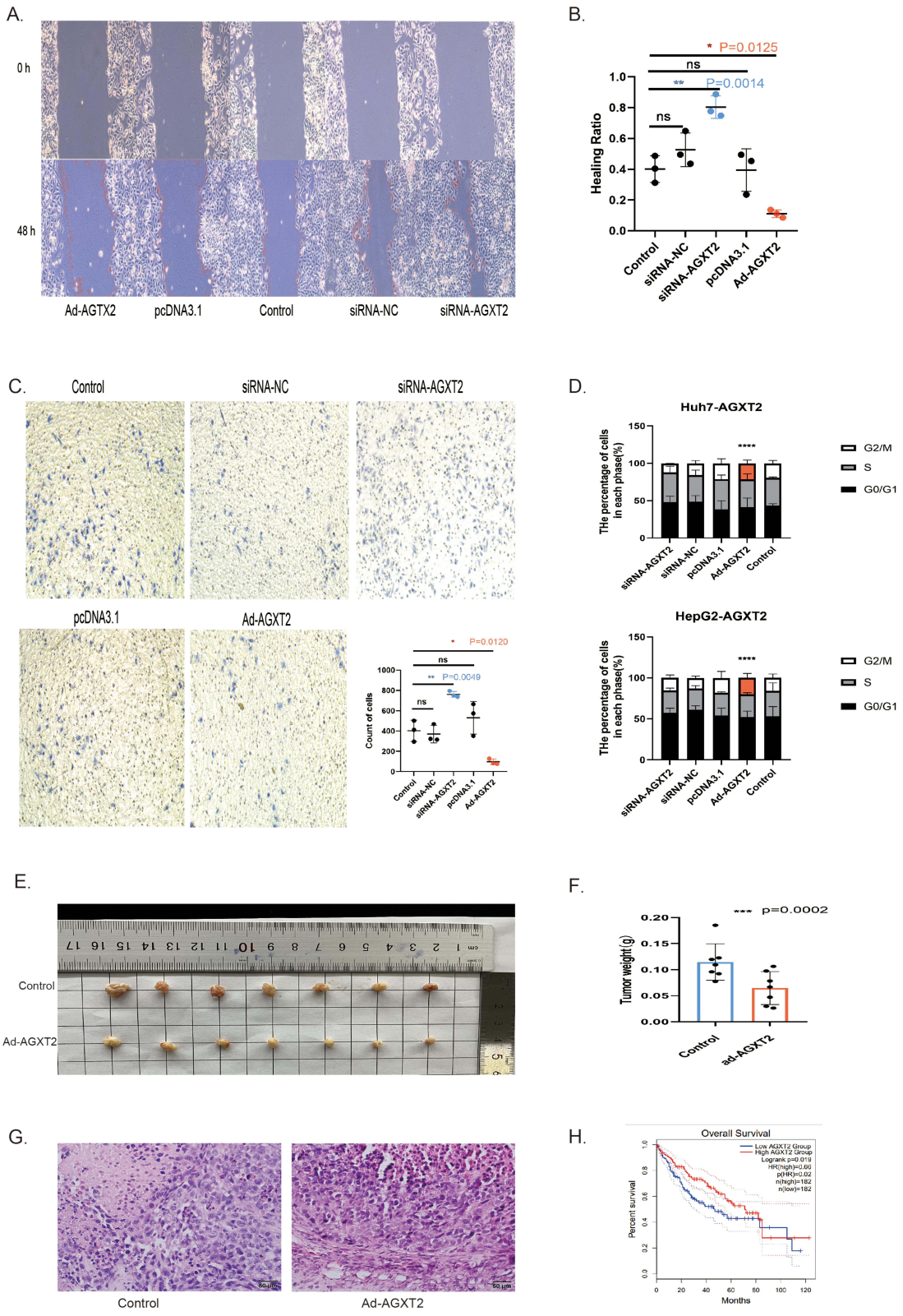

Figure 5 AGXT2 overexpression inhibited the growth and metastasis of hepatocellular carcinoma cells.(**A**).Experimental wound healing area of Huh7 cells after AGXT2 activation or inhibition. (**B**) ImageJ computer software analyzed the scratch test results. Scratch assay of Huh7 cells after activation or inhibition. Healing ratio = (Initial area - 48h area) / Initial area. (**C**) The representative images of wound healing assays in Huh7 cell lines. The invasion ability of Huh7 were measured by count of cells. (**D**) Flow cytometry was used to observe the cyclical impacts of AGXT2 overexpression and knockdown on HepG2 and Huh7 cells. (**E**) The experiment of subcutaneous tumor formation in NTG mice. (**F**) Quantitative statistical analysis of subcutaneous tumor formation in NTG mice. (**G**) HE staining of the tumor. (**H**) Low expression of AGXT2 protein indicated poor OS by GEPIA2.
Notes: Significance levels are denoted as follows: *$p \leq 0.05$, **$p \leq 0.01$, ***$p \leq 0.001$.

(Figure 5B). The transwell migration assay results showed that the siRNA-AGXT2 group had the highest number of penetrated cells ($p = 0.0049$). The number of penetrating cells in the Ad-AGXT2 group was the highest ($p = 0.0120$), and the difference was statistically significant. The results showed that the invasive ability of the cells was significantly increased after AGXT2 knockdown, while the invasive ability was decreased after AGXT2 activation (Figure 5C).

Flow cytometry analysis showed that Huh7 and HepG2 cells were blocked in the G2 phase after the overexpression of AGXT2 (Figure 5D).

Further, the NTG mice experiment revealed that the ability of subcutaneous tumor formation was reduced with AGXT2 overexpression, in contrast to the AGXT2 overexpression group and the blank Huh7 cell control group (Figure 5E). Overexpression of AGXT2 inhibited the formation of subcutaneous tumors in the NTG mice, with a statistically significant difference (Figure 5F). H&E staining was performed on the subcutaneous tumor tissues of NTG mice (Figure 5G).

The predictive significance of the AGXT2 protein in individuals with HCC was assessed in a clinical group using gene expression profiling interactive analysis (GEPIA2). Low expression of AGXT2 protein indicated poor overall survival (Figure 5H).

Discussion

Globally, primary liver cancer ranks second in terms of death rates from cancer.[20] Hepatitis B virus infection (HBV), hepatitis C virus infection (HCV), and nonalcoholic fatty liver disease are the primary culprits behind the majority of liver cancer cases.[21] Approximately 90% of liver cancer cases are HCC cases that arise due to prolonged liver inflammation.[22]

The bidirectional interaction between tumor metabolic dysregulation and epigenetics is the driving force of tumor progression.[8] Cancer is often associated with disruptions in cholesterol balance. Cholesterol is crucial in the diverse functions of cancer cells, such as regulating membrane traffic, internal signal transmission, and the synthesis of hormones and steroids.[23] In cancer cells, cholesterol metabolic reprogramming is mainly manifested by increased intracellular cholesterol synthesis, increased activity of multiple genes related to cholesterol synthesis in tumor tissues, and abnormal cholesterol accumulation in cancer tissues.[24] Cancer cells maintain the high cholesterol levels needed for rapid proliferation by increasing cholesterol biosynthesis or cellular uptake. Increased cholesterol metabolism in cancer cells can enhance the processes that lead to cancer, including the formation, movement, and growth of tumor cells.[5]

AGXT2, a versatile aminotransferase found in mitochondria, was initially discovered in 1978. The physiological importance of AGXT2 has been largely overlooked for four decades.[25] Previous research has reported that AGXT2 plays a key regulatory role in diabetes, hypertension, ischemic stroke, coronary heart disease, arteriosclerosis, fatty liver disease, and other metabolic diseases.[26–29] Currently, there is a lack of studies linking alterations in AGXT2 expression to the development of cancer and cholesterol metabolic reprogramming in HCC. Nevertheless, contemporary genomic and metabolomic research has uncovered additional roles for AGXT2.[10] Based on these studies, we speculate that AGXT2 may be involved in the metabolic reprogramming of HCC.

Through bioinformatics analysis in this study, we revealed that the expression of *AGXT2* mRNA was notably decreased in liver cancer tissues. In the HCC patients we examined, AGXT2 mRNA and protein expression were both significantly downregulated in cancer tissue compared to surrounding normal tissue by RT-qPCR and Western blot. Furthermore, AGTX2 exhibited a notable decrease in serum levels among individuals diagnosed with HCC. Moreover, the pathological immunohistochemical results of AGXT2 can be used for cancer identification by the naked eye. These results prove that AGXT2 has potential and clinical application value as a molecular diagnostic marker for HCC.

To delve deeper into the function of AGXT2 in liver cancer, we developed a cellular model with increased expression of AGTX2. Through the combined analysis of RNA-seq and UPLC-MS/MS omics, we found that AGXT2 can significantly regulate the level of cholesterol in liver cancer cells. The oil red O experiment verified the conclusion that overexpression of AGXT2 downregulated cholesterol. Cholesterol is one of the basic components of the animal cell membrane and is involved in regulating membrane fluidity and phase transition. Furthermore, cholesterol is crucial for the body's normal physiological functions, as it serves as a precursor for bioactive compounds, such as steroid hormones and bile acids.[30–32] Cholesterol and its related compounds (ancestors and byproducts) are significant factors in the development of cancer. Recent research has highlighted the role of cholesterol metabolism in controlling various tumor-

related processes, including oncogenic signaling pathways, ferroptosis, and the tumor microenvironment. Studies conducted before clinical trials have shown that inhibiting cholesterol production and absorption can hinder the development and expansion of tumors.[33]

To delve deeper into the process of cholesterol reduction, we examined the KEGG pathway and identified AGXT2 as a regulator of the cholesterol metabolism pathway. RT-qPCR and seq-RNA analysis demonstrated that *AGXT2* has the ability to increase the mRNA content of *LDLR* and *PCSK9*. Our findings show that increased expression of AGXT2 led to decreased levels of LDLR protein and increased levels of PCSK9 protein in the cholesterol metabolism pathway. Additionally, co-immunoprecipitation experiments indicated that the AGXT2 protein interacts with the LDLR protein. Major proteins carry cholesterol in the bloodstream, with LDL being taken up through endocytosis by binding to LDL receptors on the plasma membrane surface.[34] LDLR acting as a solitary transmembrane receptor, plays a role in the absorption of cholesterol and the maintenance of cholesterol balance in different cancer cells.[23,35] LDLR plays a role in the development of numerous types of cancer, and its abnormal expression have been observed in colon, prostate, lung, ovarian, breast, and liver tumors. Knocked-down LDLR could sensitize while overexpressed LDLR could insensitize epithelial ovarian cancer cells to the cytotoxic effects of cisplatin.[36] LDLR has been discovered to play a role in multiple signaling pathways, including the MAPK, NF-κB, and PI3K/Akt pathways that affect cancer cells and their nearby environment.[23] Numerous studies have verified that the hepatitis virus entry mechanism facilitated by LDLR is crucial in controlling hepatitis virus transmission, potentially influencing the development of HCC caused by hepatitis virus infection.[37,38] Studies have shown that LDLR plays a role in triggering the MAPK/ERK signaling pathway in response to HCV-E2 protein, leading to the growth of human hepatoma Huh-7 cells.[39] Increased expression of LDLR can speed up the buildup of cholesterol inside cells by enhancing the absorption of external cholesterol, potentially leading to inflammation and advancing the progression of HCC.[40,41]

PCSK9 has been recognized as a cancer inhibitor in liver cancer. PCSK9 plays a role in facilitating the entry of LDLR and LDL into lysosomes by interacting with the EGF domain of LDLR, resulting in the degradation of LDLR and ultimately lowering intracellular cholesterol levels.[42] Consistently, we found a notable decrease in PCSK9 levels and a substantial increase in LDLR levels in HCC tissues compared to neighboring liver tissues, which might have led to the enhanced absorption of external cholesterol in the liver cancer tissues.[43]

AGXT2 can reduce the transport of cholesterol into the cell by reducing the level of LDLR protein, reducing the level of intracellular cholesterol, and regulating tumor metabolism. The mechanism by which AGXT2 affects LDLR protein levels may involve two aspects. First, AGXT2 can cause LDLR protein degradation by upregulating PCSK9 protein content without affecting the *LDLR* mRNA level. Second, AGXT2 may bind directly to LDLR proteins, leading to protein degradation or other regulatory processes.

An in vivo experiment is necessary to verify the effect of the gene. As expected, our in vivo experiments revealed that AGXT2 overexpression caused stable metastases of HCC carcinoma and showed reduced tumorigenic ability in subcutaneous tumorigenesis of NTG mice compared to control mice. We also showed that AGXT2 potentially hindered the movement and penetration of liver cancer cells by disrupting the cell cycle. Thus, it appears that AGXT2 plays a role in inhibiting the growth and spread of liver cancer, as indicated by these findings from experiments conducted in living organisms in a controlled environment.

Reduced metabolic activity in neighboring tissues and increased metabolic activity in cancerous tissues result in an improved ability for liver cancer cells to utilize cholesterol, facilitating their acquisition of sufficient cholesterol from the surrounding environment to support their proliferation and expansion. Following AGXT2 overexpression, we observed the downregulation of the LDLR protein level, indicating that in HCC cells, cholesterol acquisition can be reduced by reducing LDLR-mediated intracellular cholesterol transport, thereby reducing the growth and metastasis of liver cancer tumors.

Clearly, this study demonstrated that AGXT2 could serve as a diagnostic indicator for liver cancer, validated the suppressive impact of AGXT2 in both living organisms and laboratory settings, and elucidated its potential mode of operation; however, it also highlighted certain constraints. Currently, the connection between cholesterol and the onset of liver cancer remains uncertain. Through the utilization of multi-omics sequencing and in vitro experiments, we discovered that AGXT2 has the ability to control cholesterol levels and impede the proliferation and movement of

liver cancer cells. Using AGXT2 inhibitors or knockout mice is crucial for additional validation. Future research should investigate the mechanism of AGXT2 in different liver cancer models in vivo.

Conclusion

The study determined that AGXT2 could serve as a diagnostic indicator for liver cancer and could lower intracellular cholesterol levels in liver cancer cells by controlling LDLR and PCSK9 molecules in the cholesterol metabolism pathway. Furthermore, AGXT2 was discovered to suppress the movement and penetration of HCC cells, arrest them in the G2/M phase, and hinder the development of subcutaneous tumors in NTG mice. The absence of AGXT2 in liver cancer, viewed from a mechanistic perspective, results in the buildup of cholesterol in liver cancer cells and fosters the spread and spread of cancer by triggering the cholesterol metabolism signaling pathway controlled by LDLR. In summary, AGXT2 is a novel target for the diagnosis and metabolic treatment of HCC.

Animal Studies

This study is in accordance with the protocols of the Chongqing University Three Gorges Hospital and the "Guide for the Care and Use of Laboratory Animals" of the National Institute of Health in China.

Approval of the Research Protocol

All animal experiments were performed in accordance with the protocols of the ethics committee of Chongqing University Three Gorges Hospital (file number: SXYYWD2023). The mice experiments were performed in accordance with the "Guide for the Care and Use of Laboratory Animals" of the National Institute of Health in China.

Abbreviations

AGXT, Alanine glyoxylate aminotransferase; AGXT2, Alanine glyoxylate aminotransferase 2; HCC, hepatocellular carcinoma; RT-qPCR, real-time reverse transcriptase-polymerase chain reaction; ELISA, Enzyme-linked immunosorbent assay; RNA-seq, RNA sequencing; LC-MS, liquid chromatography-mass spectrometry; UPLC-MS/MS, Ultra-high performance liquid chromatography-tandem mass spectrometry; NTG, NOD-SCID IL2Rγnull; LDLR, low density lipoprotein receptor; PCSK9, proprotein convertase subtilisin/kexin type 9; ANGPTL4, angiopoietin like 4; ADMA, Asymmetric Dimethylarginine; SDMA, Symmetric Dimethylarginine; BAIB, Beta-aminoisobutyric acid; TCGA, The Cancer Genome Atlas; GTEx, the Genotype-Tissue Expression; TPM, transcripts per million; FDR, false discovery rates; KEGG, Kyoto Encyclopedia of Genes and Genomes; GO, Gene ontology; GSEA, Gene Set Enrichment Analysis; H&E, hematoxylin and eosin; IHC, immunohistochemistry; OPLS, optimized potentials for liquid simulations; DEGs, differentially expressed genes; DETs, differentially expressed transcripts; HBV, Hepatitis B virus infection; HCV, hepatitis C virus infection.

The Accessibility of Information and Resources

The data and material generated or analyzed in this study are available upon reasonable request and could be provided by Weixian Chen (300801@cqmu. edu.cn) and Tian Chen (c13883643151@126.com).

Ethical Standards

Patient ethical approval was conducted according to the guidelines of the Declaration of Helsinki and approved by the Ethics Committee of Chongqing University Three Gorges Hospital (file number: 2023 NO.14).

Funding

The present study was supported by grants from the National Natural Science Foundation of China (No. 81873971) and the Science and Technology Commission Foundation of Chongqing (No. Cstc2021jcyj-msxmX0996, Cstb2023nscq-msx0849, and Cstc2016jcyA0264). Key Social Welfare Projects of Chongqing Wanzhou (No. wzstc-kw2023010).

Disclosure

All authors report a patent "A diagnostic marker for liver cancer and its application" issued to Chongqing University Three Gorges Hospital. The authors report no other conflicts of interest in this work.

References

1. Sung H, Ferlay J, Siegel RL, et al. Global Cancer Statistics 2020: GLOBOCAN Estimates of Incidence and Mortality Worldwide for 36 Cancers in 185 Countries. *CA Cancer J Clin*. 2021;71(3):209–249. doi:10.3322/caac.21660
2. Eslam M, Sanyal AJ, George J. International consensus p. mafld: a Consensus-driven proposed nomenclature for metabolic associated fatty liver Disease. *Gastroenterology*. 2020;158(7):1999–2014e1991. doi:10.1053/j.gastro.2019.11.312
3. Xiong J, Liu T, Mi L, et al. hnRNPU/TrkB defines a chromatin accessibility checkpoint for liver injury and nonalcoholic steatohepatitis pathogenesis. *Hepatology*. 2020;71(4):1228–1246. doi:10.1002/hep.30921
4. Valenti L, Pedica F, Colombo M. Distinctive features of hepatocellular carcinoma in non-alcoholic fatty liver disease. *Dig Liver Dis*. 2022;54 (2):154–163. doi:10.1016/j.dld.2021.06.023
5. Huang B, Song BL, Xu C. Cholesterol metabolism in cancer: mechanisms and therapeutic opportunities. *Nat Metab*. 2020;2(2):132–141. doi:10.1038/s42255-020-0174-0
6. Monroy-Ramirez HC, Galicia-Moreno M, Sandoval-Rodriguez A, Meza-Rios A, Santos A, Armendariz-Borunda J. PPARs as metabolic sensors and therapeutic targets in liver diseases. *Int J Mol Sci*. 2021;22(15):8298
7. Xiang J, Zhang Y, Tuo L, et al. Transcriptomic changes associated with PCK1 overexpression in hepatocellular carcinoma cells detected by RNA-seq. *Genes Dis*. 2020;7(1):150–159. doi:10.1016/j.gendis.2019.04.004
8. Crispo F, Condelli V, Lepore S, et al. Metabolic dysregulations and epigenetics: a bidirectional interplay that drives tumor progression. *Cells*. 2019;8(8):798
9. Li Z, Zhang H. Reprogramming of glucose, fatty acid and amino acid metabolism for cancer progression. *Cell Mol Life Sci*. 2016;73(2):377–392. doi:10.1007/s00018-015-2070-4
10. Du D, Liu C, Qin M, et al. Metabolic dysregulation and emerging therapeutical targets for hepatocellular carcinoma. *Acta Pharm Sin B*. 2022;12 (2):558–580. doi:10.1016/j.apsb.2021.09.019
11. Wang CH, Huang CW, Nguyen PA, et al. Chemopreventive effects of concomitant or individual use of statins, aspirin, metformin, and angiotensin drugs: a study using claims data of 23 million individuals. *Cancers*. 2022;14(5):1211
12. Sinn DH, Kang D, Park Y, et al. Statin use and the risk of hepatocellular carcinoma among patients with chronic hepatitis B: an emulated target trial using longitudinal nationwide population cohort data. *BMC Gastroenterol*. 2023;23(1):366. doi:10.1186/s12876-023-02996-w
13. Piekus-Slomka N, Mocan LP, Shkreli R, et al. Don't Judge a Book by Its Cover: the Role of Statins in Liver Cancer. *Cancers*. 2023;15(20). doi:10.3390/cancers15205100
14. Burdin DV, Kolobov AA, Brocker C, et al. Diabetes-linked transcription factor HNF4alpha regulates metabolism of endogenous methylarginines and beta-aminoisobutyric acid by controlling expression of alanine-glyoxylate aminotransferase 2. *Sci Rep*. 2016;6:35503. doi:10.1038/srep35503
15. Vivian J, Rao AA, Nothaft FA, et al. Toil enables reproducible, open source, big biomedical data analyses. *Nat Biotechnol*. 2017;35(4):314–316. doi:10.1038/nbt.3772
16. Villanueva A, Portela A, Sayols S, et al. DNA methylation-based prognosis and epidrivers in hepatocellular carcinoma. *Hepatology*. 2015;61 (6):1945–1956. doi:10.1002/hep.27732
17. Zhao Z, Yang H, Ji G, et al. Identification of hub genes for early detection of bone metastasis in breast cancer. *Front Endocrinol*. 2022;13:1018639. doi:10.3389/fendo.2022.1018639
18. Dunn WB, Broadhurst D, Begley P, et al. Procedures for large-scale metabolic profiling of serum and plasma using gas chromatography and liquid chromatography coupled to mass spectrometry. *Nat Protoc*. 2011;6(7):1060–1083. doi:10.1038/nprot.2011.335
19. Hammond KE, Lupo JM, Xu D, et al. Development of a robust method for generating 7.0 T multichannel phase images of the brain with application to normal volunteers and patients with neurological diseases. *Neuroimage*. 2008;39(4):1682–1692. doi:10.1016/j.neuroimage.2007.10.037
20. Bray F, Ferlay J, Soerjomataram I, Siegel RL, Torre LA, Jemal A. Global cancer statistics 2018: GLOBOCAN estimates of incidence and mortality worldwide for 36 cancers in 185 countries. *CA Cancer J Clin*. 2018;68(6):394–424. doi:10.3322/caac.21492
21. Kulik L, El-Serag HB. Epidemiology and Management of Hepatocellular Carcinoma. *Gastroenterology*. 2019;156(2):477–491e471. doi:10.1053/j.gastro.2018.08.065
22. Ringelhan M, Pfister D, O'Connor T, Pikarsky E, Heikenwalder M. The immunology of hepatocellular carcinoma. *Nat Immunol*. 2018;19 (3):222–232. doi:10.1038/s41590-018-0044-z
23. Gu J, Zhu N, Li HF, et al. Cholesterol homeostasis and cancer: a new perspective on the low-density lipoprotein receptor. *Cell Oncol Dordr*. 2022;45(5):709–728. doi:10.1007/s13402-022-00694-5
24. Li J, Gu D, Lee SS, et al. Abrogating cholesterol esterification suppresses growth and metastasis of pancreatic cancer. *Oncogene*. 2016;35 (50):6378–6388. doi:10.1038/onc.2016.168
25. Rodionov RN, Jarzebska N, Weiss N, Lentz SR. AGXT2: a promiscuous aminotransferase. *Trends Pharmacol Sci*. 2014;35(11):575–582. doi:10.1016/j.tips.2014.09.005
26. Seppala I, Kleber ME, Bevan S, et al. Associations of functional alanine-glyoxylate aminotransferase 2 gene variants with atrial fibrillation and ischemic stroke. *Sci Rep*. 2016;6:23207. doi:10.1038/srep23207
27. Zhou JP, Bai YP, Hu XL, et al. Association of the AGXT2 V140I polymorphism with risk for coronary heart disease in a Chinese population. *J Atheroscler Thromb*. 2014;21(10):1022–1030. doi:10.5551/jat.23077
28. Kayrak M, Bacaksiz A, Vatankulu MA, et al. Association between exaggerated blood pressure response to exercise and serum asymmetric dimethylarginine levels. *Circ J*. 2010;74(6):1135–1141. doi:10.1253/circj.cj-09-0419
29. Rhee EP, Ho JE, Chen MH, et al. A genome-wide association study of the human metabolome in a community-based cohort. *Cell Metab*. 2013;18 (1):130–143. doi:10.1016/j.cmet.2013.06.013

30. Schade DS, Shey L, Eaton RP. Cholesterol review: a metabolically important molecule. *Endocr Pract*. 2020;26(12):1514–1523. doi:10.4158/EP-2020-0347
31. Cardoso D, Perucha E. Cholesterol metabolism: a new molecular switch to control inflammation. *Clin Sci*. 2021;135(11):1389–1408. doi:10.1042/CS20201394
32. Rohrl C, Stangl H. Cholesterol metabolism-physiological regulation and pathophysiological deregulation by the endoplasmic reticulum. *Wien Med Wochenschr*. 2018;168(11–12):280–285. doi:10.1007/s10354-018-0626-2
33. Xu H, Zhou S, Tang Q, Xia H, Bi F. Cholesterol metabolism: new functions and therapeutic approaches in cancer. *Biochim Biophys Acta Rev Cancer*. 2020;1874(1):188394. doi:10.1016/j.bbcan.2020.188394
34. Go GW, Mani A. Low-density lipoprotein receptor (LDLR) family orchestrates cholesterol homeostasis. *Yale J Biol Med*. 2012;85(1):19–28.
35. Liu L, Sun YH, An R, Cheng RJ, Li N, Zheng JH. LDLR promotes autophagy-mediated cisplatin resistance in ovarian cancer associated with the PI3K/AKT/mTOR signaling pathway. *Kaohsiung J Med Sci*. 2023;39(8):779–788. doi:10.1002/kjm2.12696
36. Chang WC, Wang HC, Cheng WC, et al. LDLR-mediated lipidome-transcriptome reprogramming in cisplatin insensitivity. *Endocr Relat Cancer*. 2020;27(2):81–95. doi:10.1530/ERC-19-0095
37. Blanchet M, Sureau C, Guevin C, Seidah NG, Labonte P. SKI-1/S1P inhibitor PF-429242 impairs the onset of HCV infection. *Antiviral Res*. 2015;115:94–104.
38. Zeng J, Wu Y, Liao Q, Li L, Chen X, Chen X. Liver X receptors agonists impede hepatitis C virus infection in an Idol-dependent manner. *Antiviral Res*. 2012;95(3):245–256. doi:10.1016/j.antiviral.2012.06.004
39. Zhao LJ, Wang L, Ren H, et al. Hepatitis C virus E2 protein promotes human hepatoma cell proliferation through the MAPK/ERK signaling pathway via cellular receptors. *Exp Cell Res*. 2005;305(1):23–32. doi:10.1016/j.yexcr.2004.12.024
40. He M, Zhang W, Dong Y, et al. Pro-inflammation NF-kappaB signaling triggers a positive feedback via enhancing cholesterol accumulation in liver cancer cells. *J Exp Clin Cancer Res*. 2017;36(1):15. doi:10.1186/s13046-017-0490-8
41. Ma KL, Ruan XZ, Powis SH, Chen Y, Moorhead JF, Varghese Z. Inflammatory stress exacerbates lipid accumulation in hepatic cells and fatty livers of apolipoprotein E knockout mice. *Hepatology*. 2008;48(3):770–781. doi:10.1002/hep.22423
42. Sabatine MS. PCSK9 inhibitors: clinical evidence and implementation. *Nat Rev Cardiol*. 2019;16(3):155–165. doi:10.1038/s41569-018-0107-8
43. Bhat M, Skill N, Marcus V, et al. Decreased PCSK9 expression in human hepatocellular carcinoma. *BMC Gastroenterol*. 2015;15:176. doi:10.1186/s12876-015-0371-6